PERGAMON

International Journal of Heat and Mass Transfer 43 (2000) 3953–3964

International Journal of HEAT and MASS TRANSFER

www.elsevier.com/locate/ijhmt

Laminar conjugated forced convection heat transfer in curved rectangular channels

T.W. Gyves[a,*], T.F. Irvine Jr.[b]

[a]Department of Engineering, State University of New York, Maritime College, Throggs Neck, NY 10465, USA
[b]Department of Mechanical Engineering, State University of New York at Stony Brook, Stony Brook, NY 11794, USA

Received 30 April 1999; received in revised form 26 January 2000

Abstract

This paper examines fully developed laminar flow and conjugated forced convection heat transfer in curved rectangular channels. The wall average Nusselt number, $\overline{Nu}$, is presented as a function of the wall conduction parameter, ϕ, the Dean number, De, and the channel aspect ratio, λ. Secondary flow streamlines for the case of $\lambda = 1/2$ are presented to illustrate the enhanced stability in curved rectangular channels in comparison with curved square channels. A curve illustrating the relationship between ϕ_{eff}, defined as the value of ϕ at which a constant wall temperature boundary condition can be assumed, and De is presented for several values of λ. The solution for straight channels is also included, and it is found that ϕ_{eff} is independent of λ for $\lambda \leq 1/4$.

1. Introduction

Curved channel fluid flow and heat transfer analysis is encountered in many engineering problems of practical interest, including heat exchanger and turbine blade cooling passage design. As such, this topic has been accorded widespread attention in recent years. One of the more interesting aspects of curved channel flows is the introduction of a secondary flow pattern in the duct cross-section. This characteristic flow pattern is encountered in each of the three types of curved channel analyses commonly reported in the literature: isothermal flow studies (Type 1), non-isothermal flows with constant fluid density (Type 2), and non-isothermal flows with variable fluid density (Type 3). In both Type 1 and 2 systems, the secondary flow pattern results from an imbalance which develops between the centrifugal force and radial pressure fields, whereas in mixed convection flows (Type 3), gravitational and centrifugal buoyancy effects are present, further complicating the analysis of both curved channel flow field and heat transfer. The present study analyzes a Type 2 system and includes the effect of channel wall conduction, as discussed below.

A survey of previous curved channel investigations [1–19] reported in Gyves et al. [20] indicates that all of the earlier heat transfer studies have been limited by their adoption of the idealized $H1$ or $H2$ thermal boundary conditions. These boundary conditions are typically employed in order to simplify the analytical model, but they hide one of the more interesting aspects of the problem at hand, namely, the peripheral conduction which occurs in the channel wall itself. One must assume that the channel wall material has an infinitely high value of thermal conductivity in order for

* Corresponding author. Tel.: +1-718-409-7426; fax: +1-718-409-7421.
E-mail address: tgyves@sunymaritime.edu (T.W. Gyves).

0017-9310/00/$ - see front matter
PII: S0017-9310(00)00041-7

Nomenclature

a	height of a curved rectangular channel
b	width of a curved rectangular channel
C_p	specific heat
De	Dean number, $= Re(\frac{D_h}{R})^{1/2}$
D_h	hydraulic diameter, $= \frac{2a}{1+\lambda}$
dp^+/dz^+	dimensionless axial pressure gradient
f	friction factor
$\bar{h}$	average heat transfer coefficient
$H1$	constant peripheral wall temperature boundary condition
$H2$	constant peripheral heat flux boundary condition
k	thermal conductivity
l^+	dimensionless channel wall control volume spacing
n^+	dimensionless normal coordinate
$\overline{Nu}$	Nusselt number, $= \frac{\bar{h}D_h}{k_f}$, $= \frac{1}{\overline{T_w^+}-T_b^+}$
P	pressure
p^+	dimensionless pressure, $= \frac{P}{\rho\nu^2/D_h^2}$
p^*	dimensionless distance along channel perimeter, $= x^+ + y^+$
Pe	Peclet number, $= \bar{W}D_h/\alpha_f$
Pr	Prandtl number, $= \nu/\alpha$
q''	heat transferred per unit surface area of channel wall
q'''	internal heat generation per unit volume
R	radius of curvature of a curved rectangular channel
r^+	dimensionless radius of curvature, $= R/D_h$
Re	Reynolds number, $= \frac{\bar{W}D_h}{\nu_f}$, $= \overline{w^+}$
S	source term
t	duct wall thickness
T	temperature
T^+	dimensionless temperature, $= \frac{T-T_0}{q''D_h/K_f}$
U, V, W	velocity components in the X, Y, and Z-directions
u^+, v^+, w^+	dimensionless velocity components, $= (U, V, W)D_h/\nu$
$\bar{W}$	average axial velocity
$\overline{w^+}$	average dimensionless axial velocity, $= \bar{W}D_h/\nu_f$
X, Y, Z	cartesian coordinates
x^+, y^+, z^+	dimensionless coordinates, $= (X, Y, Z)/D_h$

Greek symbols

α	thermal diffusivity
Γ	diffusion coefficient in the SIMPLE algorithm
ϵ	convergence criterion use in the numerical procedure
λ	channel aspect ratio, $= a/b$
μ	dynamic viscosity
ν	kinematic viscosity
ρ	density
σ	dependent variable in the SIMPLE algorithm
ϕ	dimensionless wall conduction parameter, $= k_w t/k_f D_h$

Subscripts

b	bulk
eff	value at which $\overline{Nu} = 0.99\overline{Nu}_{H1}$
f	fluid
i, j	nodal points on numerical grid
l	local value
p	perimeter
s	value for a straight channel
T	total
w	wall
0	reference value, or cross-sectional average
σ	value corresponding to a particular dependent variable

the $H1$ condition to accurately model the system. Conversely, the $H2$ boundary condition requires that the channel wall have a zero thermal conductivity, in which case all heat generated within the wall in a specific control volume is transferred *directly* to the fluid at that same location without any peripheral conduction. Eckert and Irvine [21] noted that a wall conduction parameter, ϕ, could be employed to characterize the conjugated nature of the channel flow problem, and the present analysis provides $\overline{Nu}$ solutions for a complete range of values of this parameter, including the idealized asymptotic solutions $\overline{Nu}_{H1}$ and $\overline{Nu}_{H2}$, for several values of λ, the channel aspect ratio.

2. Analysis

The curved channel is illustrated in Fig. 1. Flow is assumed to be laminar, fully developed and steady, and all fluid properties are assumed constant. It is further assumed that the radius of curvature, R, is large compared to the channel width b. As such, the model neglects all terms of the order $1/R$ and $1/R^2$,

with the exception of the $\rho\frac{W^2}{R}$ term. The exterior channel surface is adiabatic, and the rate of internal heat generation is uniform throughout the channel walls, which are assumed to be sufficiently thin such that channel wall conduction can be modeled as one-dimensional along the channel perimeter.

The present analysis also assumes that the curved channel flow can be modeled as a parabolic flow field, which results in a significant degree of simplification in the governing equations. The dominant flow direction in curved channels is axial, and the flow can be categorized as parabolic in that direction. Convection will dominate diffusion in this direction and hence the axial diffusion terms which appear in the Navier–Stokes equations can be ignored. The fluid pressure field is assumed to be "decoupled" in parabolic flows, with the total fluid pressure at any point, P_T, considered to be the sum of a cross-stream average pressure, $P_0(Z)$, which is a function of the streamwise coordinate *alone*, and a pressure $P'(X, Y)$ which varies in the cross-stream direction. That is

$$P_T = P_0(Z) + P'(X, Y). \tag{1}$$

For fully developed flow, the axial pressure gradient, $\partial P_0/\partial Z$, is constant. Noting that

$$\frac{\partial P_T}{\partial X} = \frac{\partial P'}{\partial X} \tag{2}$$

and

$$\frac{\partial P_T}{\partial Y} = \frac{\partial P'}{\partial Y} \tag{3}$$

the governing equations for the present system can then be written in the following form [10–12] (in the equations below, P' is noted simply as P for clarity):

Continuity equation

$$\frac{\partial U}{\partial X} + \frac{\partial V}{\partial Y} = 0 \tag{4}$$

Momentum equations:

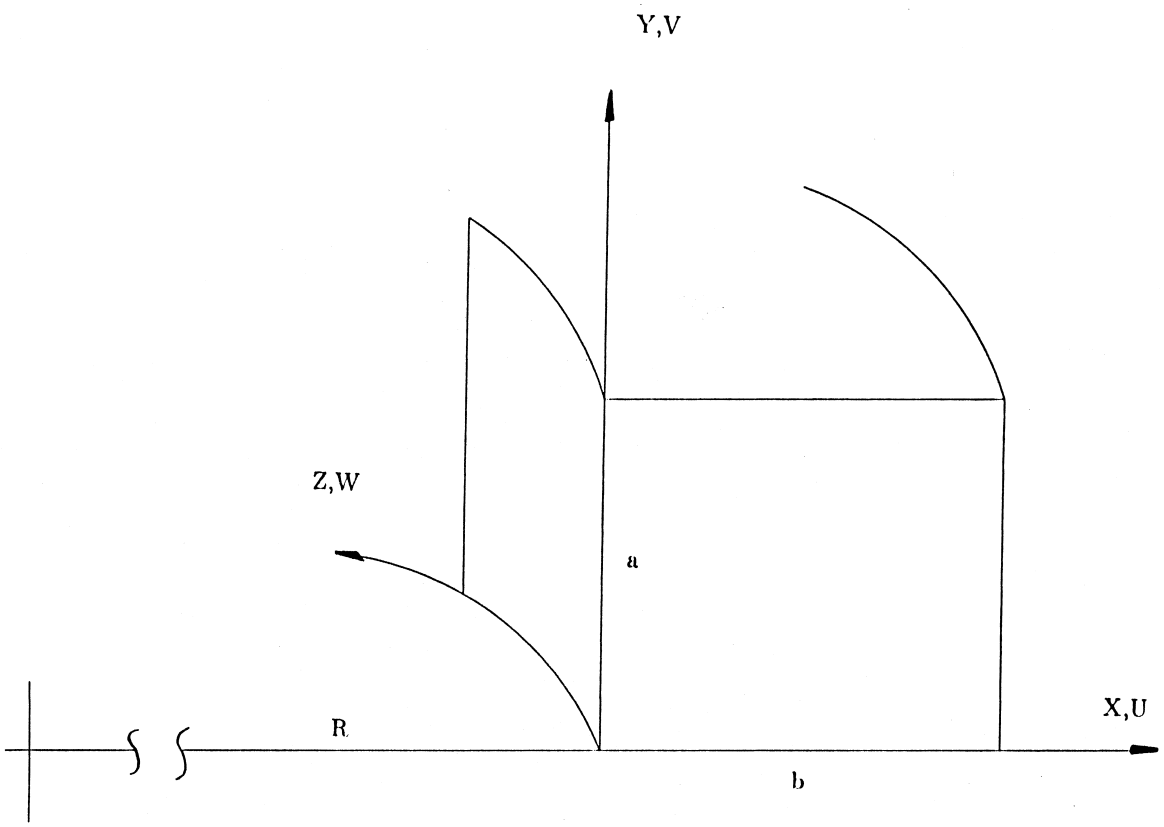

Fig. 1. Curved channel coordinate system.

$$\rho\left[U\frac{\partial U}{\partial X}+V\frac{\partial U}{\partial Y}\right]=-\frac{\partial P}{\partial X}+\rho\frac{W^2}{R}+\mu\left[\frac{\partial^2 U}{\partial X^2}+\frac{\partial^2 U}{\partial Y^2}\right] \quad (5)$$

$$\rho\left[U\frac{\partial V}{\partial X}+V\frac{\partial V}{\partial Y}\right]=-\frac{\partial P}{\partial Y}+\mu\left[\frac{\partial^2 V}{\partial X^2}+\frac{\partial^2 V}{\partial Y^2}\right] \quad (6)$$

$$\rho\left[U\frac{\partial W}{\partial X}+V\frac{\partial W}{\partial Y}\right]=-\frac{\partial P}{\partial Z}+\mu\left[\frac{\partial^2 W}{\partial X^2}+\frac{\partial^2 W}{\partial Y^2}\right] \quad (7)$$

Fluid energy equation

$$\rho C_p\left[U\frac{\partial T}{\partial X}+V\frac{\partial T}{\partial Y}+W\frac{\partial T}{\partial Z}\right]=k\left[\frac{\partial^2 T}{\partial X^2}+\frac{\partial^2 T}{\partial Y^2}\right] \quad (8)$$

Substitution of the dimensionless variables listed in the nomenclature leads to the following set of dimensionless equations:

$$\frac{\partial u^+}{\partial x^+}+\frac{\partial v^+}{\partial y^+}=0 \quad (9)$$

$$u^+\frac{\partial u^+}{\partial x^+}+v^+\frac{\partial u^+}{\partial y^+}=-\frac{\partial p^+}{\partial x^+}+\frac{w^{+2}}{r^+}+\frac{\partial^2 u^+}{\partial x^{+2}}+\frac{\partial^2 u^+}{\partial y^{+2}} \quad (10)$$

$$u^+\frac{\partial v^+}{\partial x^+}+v^+\frac{\partial v^+}{\partial y^+}=-\frac{\partial p^+}{\partial y^+}+\frac{\partial^2 v^+}{\partial x^{+2}}+\frac{\partial^2 v^+}{\partial y^{+2}} \quad (11)$$

$$u^+\frac{\partial w^+}{\partial x^+}+v^+\frac{\partial w^+}{\partial y^+}=-\frac{\partial p^+}{\partial z^+}+\frac{\partial^2 w^+}{\partial x^{+2}}+\frac{\partial^2 w^+}{\partial y^{+2}} \quad (12)$$

$$u^+\frac{\partial T^+}{\partial x^+}+v^+\frac{\partial T^+}{\partial y^+}+w^+\frac{\partial T^+}{\partial z^+}=\frac{1}{Pr}\left[\frac{\partial^2 T^+}{\partial x^{+2}}+\frac{\partial^2 T^+}{\partial y^{+2}}\right] \quad (13)$$

The equations are subject to the following boundary conditions:

At the channel wall:

$$u^+=v^+=w^+=0 \quad (14)$$

The energy equations for the channel walls are derived by balancing the net conduction across a typical control volume with the rate of internal heat generation and the convection heat transfer between the wall and fluid. For example, the left wall equation may be written as:

$$k_w t(1)\frac{d^2 T_w}{dY^2}\,dY+q'''t\,dY(1)=-k_f\,dY(1)\left(\frac{dT}{dX}\right)_{w-f} \quad (15)$$

Employing the definitions for the dimensionless temperature and the wall conduction parameter, ϕ, the left wall energy equation becomes

$$\phi\frac{d^2 T_w^+}{dy^{+2}}+1+\left(\frac{dT^+}{dx^+}\right)_{w-f}=0 \quad (16)$$

The equations for the remaining walls can be easily derived in a similar manner.

The appearance of the parameter ϕ in the wall energy equations is a direct consequence of the conjugated nature of this system. Eckert and Irvine [21] identified this important parameter in a study of convective heat transfer in triangular ducts. It is helpful at this point to examine its physical interpretation, since it plays a significant role in the analysis to follow. We have defined ϕ as

$$\phi=\frac{k_w t}{k_f D_h} \quad (17)$$

and as can be readily seen, infinitely large or small values of this parameter describe two distinct thermal boundary conditions. In the first of these (i.e. $\phi\to\infty$), the channel wall is termed "thermally thick", with k_w and/or t assuming asymptotically large values. In this case one would expect that the channel wall would act as a strong agent for conducting the heat generated in any section to neighboring areas. The result would therefore be a channel with nearly uniform wall temperatures along the entire perimeter, a situation very similar to that predicted by the $H1$ boundary condition. For asymptotically low values of ϕ (i.e., $\phi\to 0$), the channel wall is termed "thermally thin". A number of factors can contribute to such a condition, including extremely low values of k_w and t, or very large values of k_f. Poor wall conductivity, coupled with a minimal path of resistance (i.e., small t) between the wall and the fluid would result in the energy generated within the wall at any point being transfered to the fluid at that same location through convection, rather than being conducted along the wall perimeter as described in the first case above. Since the assumption is made that the internal heat generation is uniform around the

Table 1
Dimensionless conservation equation variables

σ	Γ_σ	S_σ
u	1	$S_u = w^2/r$
v	1	$S_v = 0$
w	1	$S_w = -dp/dz$
T	$1/Pr$	$S_T = -4\frac{\omega}{Re\,Pr}$

perimeter, this would result in a constant wall-to-fluid heat flux around the channel perimeter, commonly refered to as the *H2* boundary condition.

3. Numerical solution

Patankar [22] notes that the basic equation governing all analytical models of heat and mass transfer and fluid flow is a conservation equation which includes both convection and diffusion terms, as well as an appropriate source term. This general equation can be written as follows:

$$\nabla \cdot \left(\rho \bar{U} \sigma\right) = \nabla \cdot (\Gamma_\sigma \nabla \sigma) + S_\sigma \tag{18}$$

Here, $\bar{U}$ is the three-dimensional velocity vector with X, Y, and Z components, and Γ and S are the diffusion coefficient and source term, respectively, corresponding to a particular dependent variable σ. The dependent variable σ can represent dimensional or dimensionless quantities, such as a velocity component (U or u^+, as in the case of the x^+ momentum equation), or the fluid temperature (T or T^+, as in the case of the fluid energy equation). This generalized conservation equation can be written in terms of dimensionless variables, with σ representing a dimensionless dependent variable, and Γ and S the appropriate diffusion coefficient and source term, respectively. In Cartesian-tensor form, the (steady state) dimensionless conservation equation can be written as follows:

$$\frac{\partial}{\partial x_i}(u_i \sigma) = \frac{\partial}{\partial x_i}\left(\Gamma_\sigma \frac{\partial \sigma}{\partial x_i}\right) + S_\sigma \tag{19}$$

In the case of the dimensionless x-momentum equation, we have the following:

$$\sigma = u^+ \tag{20}$$

and

$$\Gamma_\sigma = 1 \tag{21}$$

The expressions for the dependent variable, σ, the diffusion coefficient, Γ_σ, and the appropriate source term, S_σ for each of the dimensionless equations are defined in Table 1.

The solution procedure employed in the present study is based upon the algorithm outlined in Patankar, working in conjunction with a new subroutine developed by Gyves [23] to account for the thermal boundary condition of peripheral wall conduction and wall-to-fluid convection. For given values of r^+, dp^+/dz^+, Pr, and ϕ, the numerical solution procedure starts with an initial guess for u^+, v^+, w^+, T^+, and p^+ at each nodal location. Updated values for all dependent parameters are then obtained using the SIMPLE algorithm, with the convective and diffusive terms formulated using a power-law scheme. The wall energy subroutine provides updated wall temperature data at each iteration. This iterative procedure is then repeated until the following convergence criterion is satisfied at each node:

$$\frac{\sigma_{i,j}^{k+1} - \sigma_{i,j}^{k}}{\sigma_{i,j}^{k+1}} < \epsilon_\sigma \tag{22}$$

where σ represents u^+, v^+, w^+, and T^+, the subscripts i, j refer to nodes on the numerical grid, and $k+1$ refers to the latest iteration. The following values for the convergence criterion, ϵ, were selected and used throughout the analysis:

$$\epsilon_{u^+,\,v^+} = 10^{-3} \tag{23}$$

$$\epsilon_{w^+,\,T^+} = 10^{-4} \tag{24}$$

These convergence parameter values are similar to those utilized by Komiyama et al. [12] and Cheng et al. [5] ($\epsilon = 10^{-3}$) and Dong and Ebadian [17] ($\epsilon = 10^{-4}$). A range of underrelaxation factors was employed during the calculation procedures to assist in obtaining a convergent solution. Values ranging from 0.25 to 0.5 were used depending upon the magnitude of De, with the smaller relaxation factors utilized at higher values of De.

The numerical results of primary interest in the present study are the calculated values for the Dean number (De), friction factor (f) and the average Nusselt number ($\overline{Nu}$). The Dean number is defined as

$$De = \frac{Re}{r^{+0.5}} \tag{25}$$

The Reynolds number, Re, which appears in this equation is based upon the cross-sectional averaged axial velocity, $\bar{W}$, calculated by integrating over the channel cross-section:

$$\bar{W} = \frac{\int W \, dx \, dy}{\int dx \, dy} \tag{26}$$

The friction factor based upon the channel hydraulic diameter, f_{D_h}, is given by

$$f_{D_h} = \frac{-2(dP/dZ)D_h}{\rho \bar{W}^2} \tag{27}$$

Applying the definitions for the dimensionless variables p^+ and z^+, it can be easily shown that the product of the friction factor and Reynolds number reduces to the following simplified expression

$$f\,Re = -2\frac{dp^+/dz^+}{\bar{w}^+} \tag{28}$$

The average wall-to-fluid heat transfer coefficient, $\bar{h}$, is defined as follows:

$$\bar{h} = \frac{q''}{\bar{T}_w - T_b} \tag{29}$$

where q'' represents the heat flux between the channel wall and the fluid, $\bar{T}_w$ is the average wall temperature around the channel perimeter, and T_b is the fluid bulk temperature. The average Nusselt number, $\overline{Nu}$, can be expressed as

$$\overline{Nu} = \frac{1}{\bar{T}_w^+ - T_b^+} \tag{30}$$

In the present analysis, $\overline{T_w^+}$ is the average wall temperature around the channel perimeter, i.e.,

$$\overline{T_w^+} = \frac{\int_p T^+ \, dl^+}{\int_p dl^+} \tag{31}$$

where dl^+ represents the wall control volume length across which a particular nodal temperature T_i^+ is assumed to be constant. The dimensionless fluid bulk temperature, T_b^+, is calculated in a manner similar to that outlined for $\bar{W}$ above, i.e.

$$T_b^+ = \frac{\int T^+ w^+ \, dx^+ dy^+}{\int w^+ \, dx^+ \, dy^+} \tag{32}$$

Numerical results for the curved channel flow field and $\overline{Nu}$ have been obtained using a curvature ratio of $r^+ = 100$ and a 30×30 numerical grid. This grid resolution is comparable to that employed by Cheng and Akiyama [10] (32×32) and Komiyama et al. [12] and Cheng et al. [5] (20×20) in their analyses of curved rectangular channels. In addition, several straight channel solutions are presented for the asymptotic case of an infinite radius of curvature (i.e., $r^+ \to \infty$). For the purposes of the present study, a straight channel is modeled using a radius of curvature of $r^+ = 1000$.

4. Results and discussion

4.1. Straight channel flow field

The accuracy of the numerical model was initially tested by examining its ability to predict straight channel behavior at asymptotically high values of the dimensionless curvature ratio, r^+, for a variety of channel aspect ratios. Table 2 provides the numerical solution for the product of $f\,Re$ for straight channels with aspect ratios ranging from $\lambda = 1.0$ to $\lambda = 1/8$, and a comparison with those solutions previously presented in the literature [24,25]. The results indicate that the numerical model is effective in calculating straight channel flow field solutions over a wide range of aspect ratios.

4.2. Straight channel forced convection ($\overline{Nu}_{H1}$ and $\overline{Nu}_{H2}$)

Straight channel $\overline{Nu}_{H1}$ and $\overline{Nu}_{H2}$ solutions have been obtained for channels with aspect ratios ranging from $\lambda = 1.0$ to $\lambda = 1/8$ for $Pr = 1.0$. The $H1$ and $H2$ solutions were obtained using values of the wall conduction parameter, ϕ, equal to 50.0 and 0.001, respectively. The numerical solutions are presented in Table 3, along with previously published solutions [24–26]. Once again, it is clear that the numerical model

Table 2
Straight channel flow field solution ($r^+ = 1000$)

	$f\,Re$		
λ	Calc.	Ref. [24,25]	%Difference
1	14.16	14.23	−0.49
4/5	14.31	14.40	−0.62
3/4	14.41	14.50	−0.62
3/5	14.91	15.50	−0.60
1/2	15.47	15.55	−0.51
1/3	16.98	17.10	−0.70
1/4	18.11	18.23	−0.66
1/5	18.93	19.10	−0.89
1/6	19.54	19.70	−0.81
1/8	20.39	20.59	−0.97

Table 3
Straight channel heat transfer solution ($r^+ = 1000$, $Pr = 1.0$)

λ	$\overline{Nu}_{H1}$			$\overline{Nu}_{H2}$		
	Calculated	Ref. [25]	%Difference	Calculated	Ref. [24,26]	%Difference
1/1	3.613	3.61	0.08	3.097	3.091	0.19
1/2	4.137	4.12	0.41	3.046	3.017	0.96
1/3	4.808	4.79	0.38	3.002	2.940	2.11
1/4	5.347	5.33	0.32	2.997	2.930	2.29
1/8	6.534	6.49	0.68	–	–	–

accurately represents straight channel behavior for $r^+ = 1000$.

4.3. Straight channel conjugated forced convection

The numerical solution for conjugated forced convection heat transfer in straight rectangular channels of various aspect ratios is illustrated in Fig. 2, where $\overline{Nu}$ is presented as a function of the wall conduction parameter, ϕ, and channel aspect ratio, λ. The data presented in Fig. 2 indicate that $\overline{Nu}$ increases with decreasing values of the aspect ratio for $\phi \geq 0.2$. This inverse relationship between $\overline{Nu}$ and λ is indicated in Table 3 for the $H1$ thermal boundary condition, and the fact that this relationship holds for nearly the entire range of ϕ values is clearly demonstrated in Fig. 2.

As noted in our earlier study [20], it is useful to introduce a parameter called the effective wall conduction parameter, ϕ_{eff}, when examining the effect of conjugated boundary conditions in systems such as that considered in the present study. This parameter provides one the opportunity to approximate the rather difficult conjugated analysis with the asymptotic solution corresponding to the thermal boundary condition of uniform peripheral wall temperature. Once again we define ϕ_{eff} as the value of ϕ at which $\overline{Nu}$ is equal to 99% of the uniform peripheral wall temperature solution, $\overline{Nu}_{H1}$. We can then infer from the actual value of ϕ whether such an approximation will yield accurate results for $\overline{Nu}$. Data for ϕ_{eff} have been obtained for channels with aspect ratios ranging from 1 to 1/8, and the results are presented in Fig. 3. Two distinct regions are depicted in this graph. In the first of these $(1/3 < \lambda < 1)$, ϕ_{eff} exhibits a strong dependence on the channel aspect ratio, with ϕ_{eff} increasing from 1.75 to 12.9 as λ decreases from 1.0 to 1/3. In the second region $(\lambda \leq 1/4)$, ϕ_{eff} is independent of the

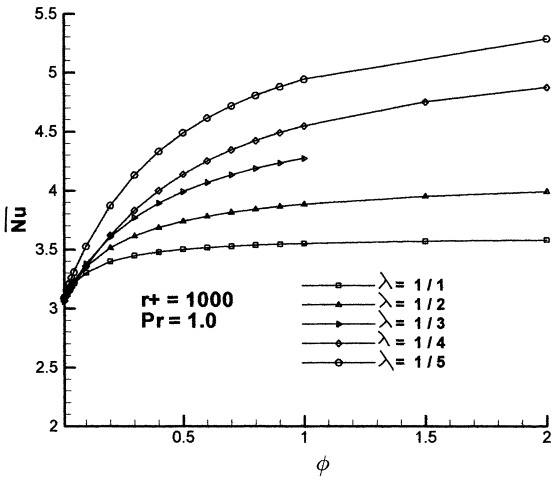

Fig. 2. Straight channel conjugated forced convection ($r^+ = 1000$, $Pr = 1.0$).

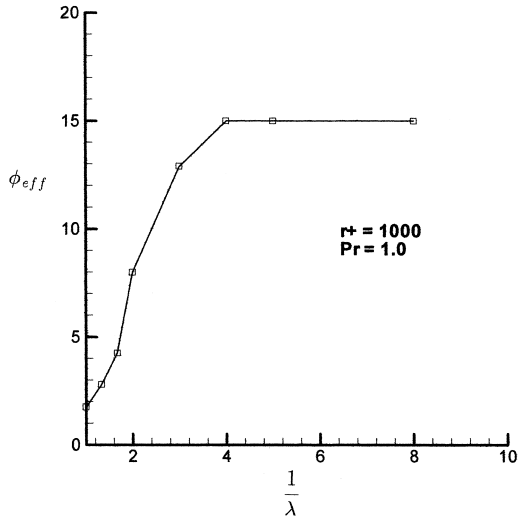

Fig. 3. Straight channel effective wall conduction parameter variation with λ ($r^+ = 1000$, $Pr = 1.0$).

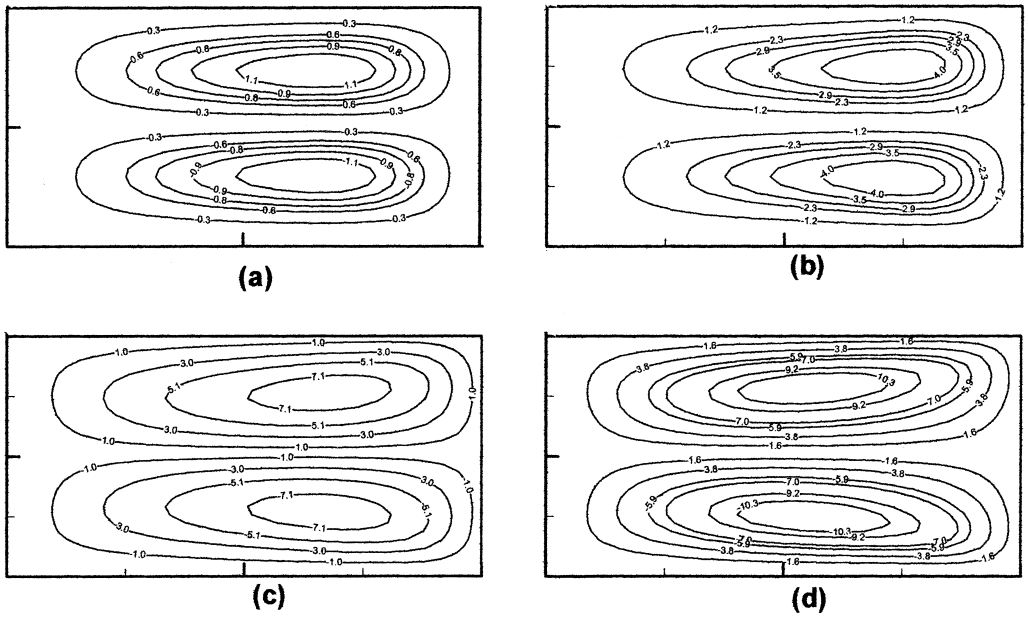

Fig. 4. Curved channel secondary flow streamlines ($r^+ = 100$, $\lambda = 1/2$): (a) $De = 31.3$; (b) $De = 69.1$; (c) $De = 115.5$; (d) $De = 183.4$. (Increasing streamline values indicate stronger secondary flow vortices.)

aspect ratio and remains constant at 15.0. This indicates that for aspect ratios less than 1/4, values of $\phi \cong 15$ are required to attain the maximum heat transfer.

4.4. Curved channel flow field

The development of a secondary cross-stream flow pattern consisting of two counter-rotating vortices at lower values of *De*, together with the subsequent transition to four vortices at higher values of *De* known as Dean's Instability, are well established phenomenon in curved channels. Fig. 4a–d illustrate the development and intensification of this secondary flow field at increasing values of *De* for a channel with $\lambda = 1/2$. It is interesting to note that the value of *De* at which the secondary flow field transitions to the four-vortex pattern is a function of the channel aspect ratio, a conclusion reached earlier by Komiyama et al. [12]. The square channel examined in Gyves et al. [20] exhibited this transition at $De = 151.1$, while the channel illustrated in Fig. 4 remains stable for $De = 183.4$, a finding similar to that presented earlier by Cheng et al. [5] for a curved channel at $De = 176$. Thus it would appear that curved rectangular channels exhibit more stable secondary cross-stream flow patterns than do square channels at equal values of *De*. The impact of channel aspect ratio on overall heat transfer rates is a key element in the present study, and will be addressed below. For the moment we simply note that it is the introduction of a secondary flow field and the sub-

Table 4
Curved channel flow field solution ($r^+ = 100$, $\lambda = 1/2$)

dp/dz^+	*De*			*f Re*/*f Re*$_s$		
	Calculated	Ref. [5]	%Difference	Calculated	Ref. [5]	%Difference
−5000	16.1	16.0	0.63	1.003	1.01	−0.69
−10,000	31.3	31.1	0.64	10.3	1.04	−0.96
−26,000	69.1	68.1	1.47	1.22	1.24	−1.61
−50,000	115.5	112.6	2.58	1.40	1.44	−2.78
−90,000	183.4	176.6	3.85	1.59	1.65	−3.64

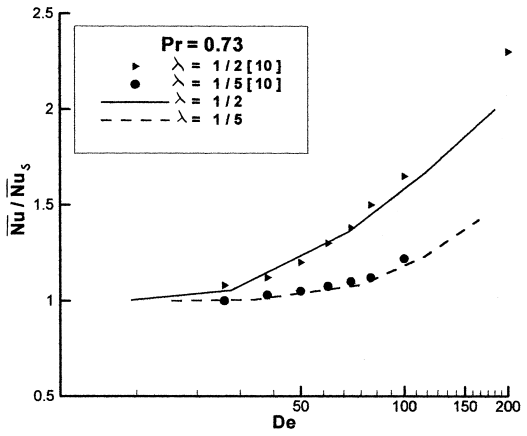

Fig. 5. Curved channel forced convection — $H1$ boundary condition ($r^+ = 100$, $Pr = 0.73$).

sequent onset of Dean's Instability which serves to produce increased heat transfer rates in curved channels above those found in straight channels. For equal values of De, then, one would expect to see a decrease in the value of $\overline{Nu}/\overline{Nu}_s$ as the channel aspect ratio decreases from 1.0. This is in fact what our findings indicate, as will be discussed below.

The solutions for the Dean Number and the friction factor ratio (i.e., the ratio of the curved channel $f\,Re$ to the straight channel $f\,Re_s$) at various values of the axial pressure gradient are presented in Table 4 for a channel with $\lambda = 1/2$, and are found to be in good agreement with data presented earlier by Cheng et al. [5].

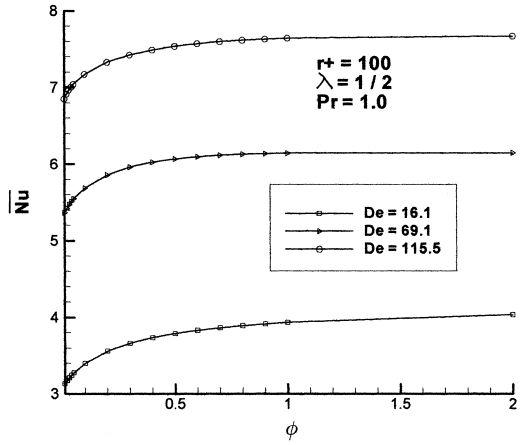

Fig. 6. Curved channel conjugated forced convection ($r^+ = 100$, $\lambda = 1/2$, $Pr = 1.0$).

4.5. Curved channel forced convection (H1 boundary condition)

As noted above, all prior studies of forced convection heat transfer in curved rectangular channels have employed one or more of the simplified thermal boundary conditions, including the $H1$ boundary condition which assumes a peripherally uniform wall temperature. The present analysis yielded results for $\overline{Nu}_{H1}/\overline{Nu}_s$, which are in good agreement with data presented earlier by Cheng and Akiyama [10] for several aspect ratios, as indicated in Fig. 5.

One of the more interesting results presented in Fig. 5 has already been alluded to with respect to the stability of the secondary flow stream in curved channels with aspect ratios other than $\lambda = 1$. It was noted above that as the value of λ decreases from 1.0, the transition to a four vortex secondary flow is delayed until progressively higher values of De are reached. The impact of this is clearly seen in Fig. 5, where for fixed values of De, the ratio of $\overline{Nu}_{H1}/\overline{Nu}_s$ decreases as the aspect ratio decreases from $\lambda = 1.0$. Alternately, one can see that the rate of increase of the curved channel $\overline{Nu}_{H1}$ over the straight channel value is significantly reduced as the aspect ratio decreases from $\lambda = 1/2$ to $\lambda = 1/5$. These results are also in qualitative agreement with data presented by Komiyama et al. [12] for curved channels with similar aspect ratios and $Pr = 0.71$.

4.6. Curved channel conjugated forced convection

The solution to conjugated forced convection in a curved rectangular channel with $\lambda = 1/2$ is presented in Fig. 6, where $\overline{Nu}$ is presented as a function of both ϕ and De for $Pr = 1.0$. The dramatic increase in $\overline{Nu}$ with increased values of De is a direct result of the presence of the secondary flow field. It is also clear that the introduction of the secondary flow vortices greatly enhances the rate of heat transfer over that found in straight channels, irrespective of the thermal boundary condition imposed upon the system. This is evident

Table 5
Curved channel conjugated heat transfer solution ($r^+ = 100$, $\lambda = 1/2$, $Pr = 1.0$)

dp/dz^+	De	$\overline{Nu}_{H2}$	$\overline{Nu}_{H1}$	Nu/Nu_s	ϕ_{eff}
−5000	16.1	3.13	4.17	1.01	6.50
−10,000	31.3	3.54	4.46	1.08	4.00
−26,000	69.1	5.37	6.15	1.49	0.60
−50,000	115.5	6.85	7.67	1.85	0.70
−90,000	183.4	8.55	9.34	2.26	0.60

Table 6
Curved channel conjugated heat transfer solution ($r^+ = 100$, $\lambda = 1/3$, $Pr = 1.0$)

dp/dz^+	De	$\overline{Nu}_{H1}$	Nu/Nu_s	ϕ_{eff}
−5000	14.72	4.812	1.001	10.80
−8000	23.49	4.846	1.008	10.00
−10,000	29.24	4.903	1.020	9.70
−14,000	40.25	5.110	1.063	7.25
−20,000	55.17	5.576	1.160	2.40
−30,000	76.71	6.492	1.350	0.68
−40,000	96.01	7.280	1.514	0.60
−50,000	114.09	7.895	1.642	0.60

when one compares the straight channel conjugated solution for $\overline{Nu}$ for $\lambda = 1/2$ presented in Fig. 2 with the data in Fig. 6.

The curvature-induced secondary flow field also has a dramatic effect on the value of ϕ_{eff}, as indicated in Tables 5 and 6 for channels with $\lambda = 1/2$ and $\lambda = 1/3$. For all aspect ratios examined in the present study, the value of ϕ_{eff} decreases as De increases. This is similar to our earlier findings for square channels [20], where ϕ_{eff} was shown to decrease from a straight channel value of 1.75 to a value of 0.3 for $De > 30$. In Fig. 7 ϕ_{eff} is presented as a function of De for $\lambda = 1$, 1/2, and 1/3. Here we note the very interesting result that, for $\phi_{eff} \sim 0.6$ and $De > 80$, the forced convection $\overline{Nu}$ is very closely approximated by the $\overline{Nu}_{H1}$ solution for $\lambda = 1$, 1/2, and 1/3. As such, very reasonable accuracy can be obtained under these specific conditions by employing the simplified boundary condition of uniform peripheral wall temperature, thereby eliminating the need to perform the more rigorous conjugated analysis.

The influence of aspect ratio on local heat transfer rates around the curved channel perimeter for fixed De values is illustrated in Fig. 8. Here, the local Nusselt number, defined as

$$Nu_l = \frac{1}{T_w^+ - T_b^+}\left(\frac{dT^+}{dn^+}\right) \tag{33}$$

is plotted as a function of location around the channel perimeter for channels with $\lambda = 1$, 1/2, and 1/3, with $De = 100.9$, 101.6, and 100.6 respectively. The dimensionless distance around the channel perimeter, p^*, is measured in a counter-clockwise fashion starting at the bottom left corner. For a thermal boundary condition of $\phi = 1.0$, we note the dramatic rise in the maximum Nu_l value along the outer wall as the aspect ratio decreases from $\lambda = 1$ to 1/3. The point of maximum heat transfer also shifts to the center of the outer wall for non-square curved channels, whereas the square channel's maximum $\overline{Nu}_l$ value is located at two points slightly above and below the channel's horizontal centerline. This trend towards higher local heat transfer rates at decreasing values of λ is reversed along the inner wall, where it can be seen that Nu_l values decrease as λ decreases. The profile along the inner wall maintains its form for all aspect ratios, with the points of maximum Nu_l located symmetrically about the horizontal centerline. Local heat transfer rates along the top and bottom walls are observed to be identical for a given value of λ, and show a less marked increase for decreasing λ than that noted above for the outer wall. For each value of λ examined, the maximum Nu_l value for the top and bottom walls is located to the right of the channel's vertical centerline.

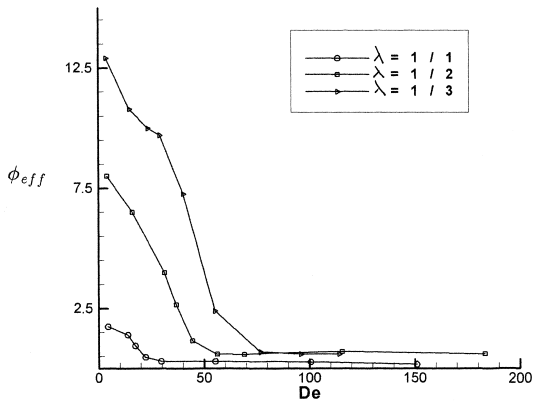

Fig. 7. Curved channel effective wall conduction parameter variation with De ($r^+ = 100$, $Pr = 1.0$).

5. Conclusions

The numerical solution to conjugated forced convection in curved rectangular channels has been presented here for the first time, and the asymptotic straight channel solutions for $\phi \to 0(H2)$ and $\phi \to \infty(H1)$ have been shown to be in strong agreement with data reported previously in the literature for channel aspect ratios ranging from $\lambda = 1$ to $\lambda = 1/8$. The dramatic increase in $\overline{Nu}$ with increasing De has been demonstrated for all values of the wall conduction parameter ϕ. It has been shown, however, that this curvature effect is less significant as the channel aspect ratio decreases from $\lambda = 1$, due to a delay in the transition to a four-vortex flow pattern. The effective wall conduction parameter, ϕ_{eff}, has been shown to be strongly dependent upon the channel aspect ratio in straight channels for $1/3 < \lambda < 1$, and independent of λ in straight channels with $\lambda \leq 1/4(\phi_{eff} = 15)$, as well as in curved channels with $De \geq 100(\phi_{eff} \approx 0.6)$.

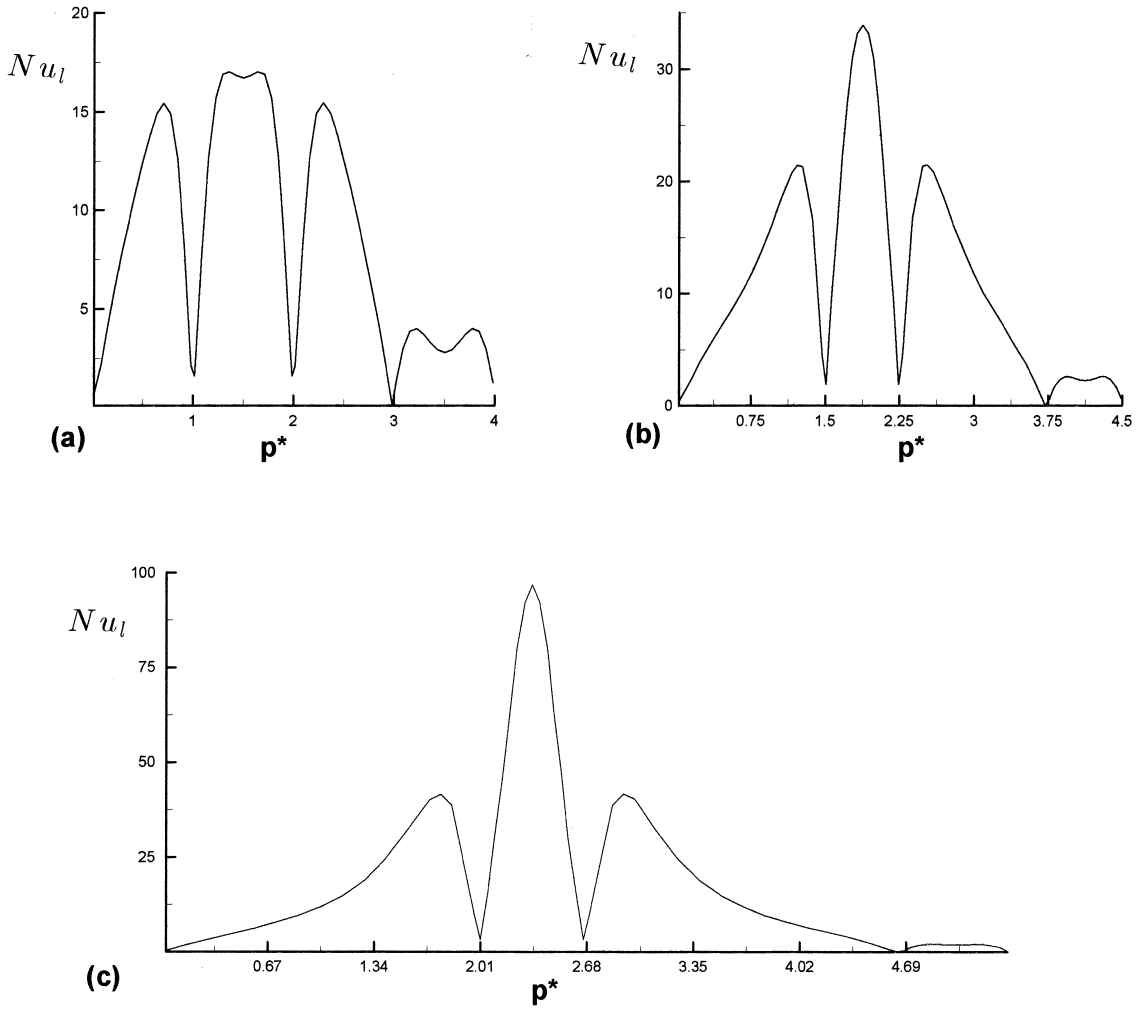

Fig. 8. Curved channel local Nusselt number variation with $\lambda(r^+ = 100,\ Pr = 1.0,\ \phi = 1.0)$: (a) $\lambda = 1$, $De = 100.9$; (b) $\lambda = 1/2$, $De = 101.6$; (c) $\lambda = 1/3$, $De = 100.6$.

References

[1] J. Eustice, Flow of water in curved pipes, Proceedings of the Royal Society of London, Ser. A. 84 (1910) 107–118.

[2] J. Eustice, Experiments on streamline motion in curved pipes, Proceedings of the Royal Society of London, Ser. A. 85 (1911) 119–131.

[3] W.R. Dean, Note on the motion of fluid in a curved pipe, Philosophy Magazine 20 (1927) 208–223.

[4] W.R. Dean, The stream-line motion of fluid in a curved pipe, Philosophy Magazine 30 (1928) 673–695.

[5] K.C. Cheng, R.C. Lin, J.W. Ou, Fully developed laminar flow in curved rectangular channels, ASME Journal of Fluids Engineering 98 (1976) 41–48.

[6] S. Thangam, N. Hur, Laminar secondary flows in curved rectangular ducts, Journal of Fluid Mechanics 217 (1990) 421–440.

[7] K.N. Ghia, J.S. Sokhey, Laminar incompressible viscous flow in curved ducts of regular cross-sections, ASME Journal of Fluids Engineering 99 (1977) 640–648.

[8] Y. Mori, W. Nakayama, Study on forced convective heat transfer in curved pipes, International Journal of Heat and Mass Transfer 10 (1967) 681–695.

[9] Y. Mori, Y. Uchida, T. Ukon, Forced convective heat transfer in a curved channel with a square cross section, International Journal of Heat and Mass Transfer 14 (1971) 1787–1805.

[10] K.C. Cheng, M. Akiyama, Laminar forced convection heat transfer in curved rectangular channels, International Journal of Heat and Mass Transfer 13 (1970) 471–490.

[11] Z. Zapryanov, C. Christov, E. Toshev, Fully developed laminar flow and heat transfer in curved tubes, International Journal of Heat and Mass Transfer 23 (1980) 873–880.
[12] Y. Komiyama, F. Mikami, K. Okui, T. Hori, Laminar forced convection heat transfer in curved channels of rectangular cross section, Heat Transfer Japanese Research 12 (2) (1984) 68–91.
[13] G.J. Hwang, C.H. Chao, Forced laminar convection in a curved isothermal square duct, ASME Journal of Heat Transfer 113 (1991) 48–55.
[14] L.S. Yao, S.A. Berger, Flow in heated curved pipes, Journal of Fluid Mechanics 88 (1978) 339–354.
[15] J. Prusa, L.S. Yao, Numerical solution for fully developed flow in heated curved tubes, Journal of Fluid Mechanics 123 (1982) 503–522.
[16] J.B. Lee, H.A. Simon, J.C.F. Chow, Buoyancy in developed laminar curved tube flows, International Journal of Heat and Mass Transfer 28 (3) (1985) 631–640.
[17] Z.F. Dong, M.A. Ebadian, Effects of buoyancy on laminar flow in curved elliptic ducts, ASME Journal of Heat Transfer 114 (1992) 936–943.
[18] R. Sankar, K. Nandakumar, J.H. Masliyah, Mixed convection in heated curved square ducts, in: Proceedings of the Eighth International Heat Transfer Conference, 1986, pp. 1407–1412.
[19] D.J. Goering, J.A.C. Humphrey, R. Greif, The dual influence of curvature and buoyancy in fully developed tube flows, International Journal of Heat and Mass Transfer 40 (9) (1997) 2187–2199.
[20] T.W. Gyves, T.F. Irvine Jr., M.H.N. Naraghi, Gravitational and centrifugal buoyancy effects in curved square channels with conjugated boundary conditions, International Journal of Heat and Mass Transfer 42 (11) (1999) 2015–2029.
[21] E.R.G. Eckert, T.F. Irvine Jr., Pressure drop and heat transfer in a duct with triangular cross section, ASME Journal of Heat Transfer (1960) 125–138.
[22] S.V. Patankar, Numerical Heat Transfer and Fluid Flow, Hemisphere, Washington, DC, 1980.
[23] T.W. Gyves, A numerical solution to conjugated mixed convection heat transfer in curved square channels, Ph.D. Thesis, State University of New York at Stony Brook, Stony Brook, NY, 1997.
[24] R.K. Shah, A.L. London, Thermal boundary conditions and some solutions for laminar duct flow forced convection, ASME Journal of Heat Transfer 96 (1974) 159–165.
[25] W.M. Kays, M.E. Crawford, Convective Heat and Mass Transfer, McGraw-Hill, New York, 1980.
[26] R.K. Shah, A.L. London, Laminar flow forced convection in ducts, in: T.F. Irvine Jr., J.P. Hartnett (Eds.), Advances in Heat Transfer, Academic Press, New York, 1978.